Journal of Visualized Experiments

A Label-Free Segmentation Approach for Intravital Imaging of Mammary Tumor Microenvironment

--Manuscript Draft--

Article Type:	Invited Methods Collection - JoVE Produced Video
Manuscript Number:	JoVE63413R2
Full Title:	A Label-Free Segmentation Approach for Intravital Imaging of Mammary Tumor Microenvironment
Corresponding Author:	Suzanne Ponik, PhD University of Wisconsin-Madison School of Medicine and Public Health Madison, WI UNITED STATES
Corresponding Author's Institution:	University of Wisconsin-Madison School of Medicine and Public Health
Corresponding Author E-Mail:	ponik@wisc.edu
Order of Authors:	Suzanne Ponik, PhD
	Brian Burkel
	David Inman
	Maria Virumbrales-Munoz
	Erica Hoffmann
Additional Information:	
Question	**Response**
Please specify the section of the submitted manuscript.	Cancer Research
Please indicate whether this article will be Standard Access or Open Access.	Standard Access ($1400)
Please indicate the **city, state/province, and country** where this article will be **filmed**. Please do not use abbreviations.	Madison, WI USA
Please confirm that you have read and agree to the terms and conditions of the author license agreement that applies below:	I agree to the Author License Agreement
Please confirm that you have read and agree to the terms and conditions of the video release that applies below:	I agree to the Video Release
Please provide any comments to the journal here.	

TITLE:

A Label-Free Segmentation Approach for Intravital Imaging of Mammary Tumor Microenvironment

AUTHORS AND AFFILIATIONS:

Brian M. Burkel[1], David R. Inman[1], María Virumbrales-Muñoz[1,2], Erica J. Hoffmann[1], Suzanne M. Ponik[1,3]

Email addresses of co-authors:

Brian M. Burkel	(bmburkel@wisc.edu)
David R. Inman	(drinman@wisc.edu)
María Virumbrales-Muñoz	(virumbralesm@wisc.edu)
Erica J. Hoffmann	(ejhoffmann@wisc.edu)
Suzanne M. Ponik	(ponik@wisc.edu)

Corresponding author:

Suzanne M. Ponik	(ponik@wisc.edu)

SUMMARY:

The intravital imaging method described here utilizes collagen second harmonic generation and endogenous fluorescence from the metabolic co-factor NAD(P)H to non-invasively segment an unlabeled tumor microenvironment into tumor, stromal, and vascular compartments for in-depth analysis of 4D intravital images.

ABSTRACT:

The ability to visualize complex and dynamic physiological interactions between numerous cell types and the extracellular matrix (ECM) within a live tumor microenvironment is an important step toward understanding mechanisms that regulate tumor progression. While this can be accomplished through current intravital imaging techniques, it remains challenging due to the heterogeneous nature of tissues and the need for spatial context within the experimental observation. To this end, we have developed an intravital imaging workflow that pairs collagen second harmonic generation imaging, endogenous fluorescence from the metabolic co-factor NAD(P)H, and fluorescence lifetime imaging microscopy (FLIM) as a means to non-invasively compartmentalize the tumor microenvironment into basic domains of the tumor nest, the surrounding stroma or ECM, and the vasculature. This non-invasive protocol details the step-by-step process ranging from the acquisition of time-lapse images of mammary tumor models to post-processing analysis and image segmentation. The primary advantage of this workflow is that it exploits metabolic signatures to contextualize the dynamically changing live tumor microenvironment without the use of exogenous fluorescent labels, making it advantageous for human patient-derived xenograft (PDX) models and future clinical use where extrinsic fluorophores are not readily applicable.

INTRODUCTION:

The extracellular matrix (ECM) in the tumor microenvironment is known to be dynamically

deposited and remodeled by multiple cell types to further facilitate disease progression[1–3]. These matrix alterations provide both mechanical and biological cues that alter cell behavior and often result in a continuing cycle of matrix remodeling[4]. Investigation into the dynamic, reciprocal interplay between tumor cells and the extracellular matrix is often conducted using three-dimensional (3D) *in vitro* culture or microfluidic systems. While these bottom-up approaches have demonstrated mechanisms of ECM remodeling[5–7], increased proliferation[8], epithelial to mesenchymal transition[9–12], and tumor cell migration and invasion[7, 13–16], their focus has been primarily on a few cell types (e.g., tumor cells or fibroblasts) within a homogeneous 3D matrix compared to the diversity and heterogeneity of interactions present within a physiological tissue. In addition to *in vitro* systems, *ex vivo* tumor histology can also provide some insight into these cell-cell and cell-ECM interactions[17]. Immunohistochemistry has the advantage of being able to analyze multiple cell types with respect to the spatially heterogeneous composition and architecture of the ECM, but the static endpoints of fixed tissue do not capture the dynamic nature of interactions between cells and the microenvironment.

The use of intravital imaging has opened the door to interrogate live interactions within the spatial and temporal context of the native tumor microenvironment, and the capabilities of intravital tumor imaging are advancing rapidly. Improvements in the design of imaging windows and surgical techniques to implant the windows have enabled long-term longitudinal tumor imaging at a variety of anatomical locations i.e., primary tumor, lymph nodes, metastatic sites[18–20]. Moreover, the capacity of optical instrumentation to visualize and collect data in multiple dimensions (i.e., spectral, spatial fluorescence intensity), and lifetime and at high resolution and speed (video rate) is becoming widely accessible. The improved technology provides an opportunity to explore rapid changes in cell signaling and phenotypic dynamics within a physiological environment. Lastly, the expansion of optogenetic tools and the wide array of genetic fluorescent constructs allow for the tagging of specific cell types to capture cell migration in the tumor microenvironment or cell lineage tracing during development or disease progression[21, 22]. The use of these tools in combination with CRISPR/Cas9 technology provides researchers the opportunity to generate unique animal models in a timely manner.

While all these advances make intravital imaging an increasingly powerful method to explore dynamic and physiological cellular interactions, there is still an important need to develop strategies that provide spatial, temporal, and structural context at the tissue level to these biological interactions. Currently, many intravital imaging studies compensate for the lack of visual landmarks such as blood vessels by injecting fluorescent dyes into the vasculature or employing mouse models that exogenously express fluorescent proteins to delineate physical features. Injectable dyes and substrates like fluorescent dextrans are broadly utilized to successfully label the vasculature in intravital collections[19, 23, 24]. However, this approach is not without limitations. For one, it requires additional mouse manipulations and its utility is limited to short-term experiments. For longitudinal studies, fluorescent dextran can be problematic as we observe the accumulation of dextran in phagocytic cells or diffusion into the surrounding tissue over time[25]. Exogenous fluorescent protein incorporation into the mouse model has been presented as an alternative to fluorescent dextrans but presents limitations of its own. The availability and diversity of exogenous fluorophores within mouse models are still limited and

expensive to create. Additionally, in specific models, such as PDX models, genetic manipulations are not desirable or possible. It has also been shown that the presence of fluorescent or bioluminescent proteins within cells are recognized as foreign within the mouse, and within immunocompetent mouse models, this reduces the amount of metastasis due to the response of the host immune system[26, 27]. Lastly, exogenous fluorescent proteins or fluorescent dyes used for spatial context or to segment subsequent data often occupy prime ranges of the light spectrum that could otherwise be used to investigate the physiological interactions of interest.

The use of the intrinsic signal from the ECM or endogenous fluorescence from cells within the tissue can not only be a useful tool to characterize cell behavior or specific physiological structures but also a universal means to segment the data for more in-depth cellular and spatial analysis. Second harmonic generation (SHG) has long been used to visualize the ECM[28]. With the subsequent development of important tools to aid in the characterization of fiber organization[29–31], it is possible to characterize cell behavior relative to local ECM structure. In addition, autofluorescence from the endogenous metabolite, NAD(P)H, provides another label-free tool to compartmentalize the tumor microenvironment *in vivo*. NAD(P)H fluoresces brightly in tumor cells and can be used to discriminate the boundaries of the growing tumor nest from its surrounding stroma[21, 32]. Lastly, the vasculature is an important physiological structure in the tumor microenvironment and the site of key cell-type-specific interactions[33–35]. The excitation of red blood cells (RBC) or blood plasma has been used to visualize the tumor vasculature, and using two- or three-photon excitation (2P; 3P) the measurement of blood flow rates has been shown to be possible[36]. However, while larger blood vessels are easily identifiable by their endogenous fluorescence signatures, the identification of subtle, variable, and less fluorescent small blood vessels requires more expertise. These inherent difficulties hinder optimal image segmentation. Fortunately, these sources of endogenous fluorescence (i.e., red blood cells and blood plasma) can also be measured by fluorescence lifetime imaging[37], which capitalizes on the unique photophysical properties of the vasculature and represents a useful addition to the growing intravital toolbox.

In this protocol, a workflow for the investigation of four-dimensional (4D) intravital imaging, from acquisition to analysis, explicitly using intrinsic signals like endogenous fluorescence and SHG is described. This protocol is specifically written for longitudinal studies through a mammary imaging window where exogenous fluorescence may not be practical or possible, as is the case with PDX models. The segmentation principles outlined here, however, are broadly applicable to intravital users investigating tumor biology, tissue development, or even normal tissue physiology. The reported suite of analysis approaches will allow the users to differentiate cellular behavior between regions of aligned or random collagen fiber configurations, compare numbers or behaviors of cells residing in specific regions of the tumor microenvironment, and map the vasculature to the tumor microenvironment using only label-free or intrinsic signal. Together, these methods create an operational framework for maximizing the depth of information gained from 4D intravital imaging of the mammary gland while minimizing the need for additional exogenous labels.

PROTOCOL:

All experiments described were approved by the University of Wisconsin-Madison's Institutional Animal Care and Use Committee. The well-being and pain management in all animal experiments is paramount. Thus, every effort is made to make sure the animal is comfortable and well-cared for at each step of the procedure.

1. Generation of the mammary imaging window (MIW)

1.1 To construct the mammary imaging window, fabricate a 14 mm ring from surgical grade stainless steel.

1.2 Clean the machined window frame using a hot solution of 5% cleaning detergent, rinse for 10 min under running deionized water (DI) water, soak in 100% ethanol for 10 min, and then dry under a heat lamp. Autoclave the dried MIW frame and store it for later use.

1.3 Prepare MIW cover glass as follows. Soak the #1.5 12 mm round cover glass in 100% ethanol for 10 min, dry under a heat lamp, and then secure to the metal MIW frame using cyanoacrylate adhesive. Cure the adhesive overnight.

1.4 Clean the assembled MIW of excess adhesive using an acetone soaked swab, and disinfect by submerging it in 70% ethanol for at least 1 min. Allow the cleaned window to dry. Prepare the MIW in advance and store it in a sterile Petri dish prior to surgical implantation.

2. Surgical implantation of the MIW

2.1 Autoclave surgical tools and sanitize surfaces with 70% ethanol before beginning the surgery for the window implantation.

2.2 Perform surgery on a sanitized tabletop using a warming blanket covered with a sterile field. Set the warming blanket such that the temperature measured on top of the sterile field is 40 °C.

2.3 Use auxiliary cold lighting to help prevent tissue drying. Use magnifying glasses to facilitate the surgical procedure. Wear PPE consisting of a sterile, single-use lab coat, surgical sleeves, gloves, eye protection, and face mask as recommended by the surgical best practices.

2.4 Anesthetize the mouse using an anesthesia vaporizer machine with an isoflurane setting of 2.0% and flow rate of 2.0 L/min. Administer analgesic (10 mg/kg meloxicam) by subcutaneous injection.

NOTE: Provide additional doses within the first 24 h, preferably every 8–12 h for the first 2 days after surgery.

2.5 Once anesthetized (confirmed by no response to toe-pinch), apply a moisturizing eye gel to prevent drying of the eyes. Use a depilatory cream to remove fur at the surgery site (4th inguinal mammary gland) followed by rinsing with sterile water-soaked gauze.

2.6 Prepare the depilated surgical site for surgery by sanitizing the skin surface with 3 alternating betadine and ethanol scrubs.

2.7 To begin the surgery, gently lift the skin over mammary gland number 4 using forceps. Once the skin is pulled away from the body wall, remove a ~1 mm section of the dermal layer at the tip of the forceps with surgical micro-scissors. If bleeding occurs, apply gentle pressure with sterile gauze until the bleeding stops.

NOTE: In general, larger tumors have a greater potential to bleed than smaller tumors or normal tissues.

2.8 Detach the mammary gland from the dermal layer with gentle forceps movements at the surgical opening to avoid cutting which will remove more of the dermal.

2.9 Create a 10 mm incision and release the mammary gland from the dermal layer at the periphery so that sutures can be placed without penetrating the mammary gland. Add PBS to cover the exposed gland/tumor and to prevent drying.

2.10 Create a purse-string suture along the periphery of the opening using 5-0 silk braided suture. Insert an edge of the MIW so that the dermal layer engages into the receiving notch of the MIW.

2.11 Gently stretch the epithelium at the opposite side of the MIW and push the metal MIW into place such that the dermal layer fully engages the receiving notch around the entire MIW circumference. Cinch the purse string tight to draw the dermal layer into the notch and tie it off to fully secure the window.

2.12 Add a topical antibiotic to the dermal layer at the MIW, and continuously monitor the mouse until it has regained sufficient consciousness to maintain sternal recumbency. House the MIW-implanted mice separately on soft bedding with an igloo placed in the cage, and allow the mouse to recover for 48 h before imaging.

3. Positioning and maintaining mouse on the microscope stage for imaging

3.1 Set up the heating chamber on the microscope stage. Use a forced-air system set to 30 °C or any other similar system. Use an additional objective heater to avoid drift in z focus. Allow the system to come to equilibrium for at least 1 h before imaging.

NOTE: Anesthetized mice are incapable of properly maintaining their body temperature, and therefore, it is necessary to have a heated environment for any time-lapse acquisitions**.** The

objective heater helps to combat the effects of thermal expansion, a phenomenon that causes drift in z focus as the objective lens and the tissue being imaged come to thermal equilibrium.

3.2 Once the heating chamber on the microscope has stabilized at 30 °C, anesthetize the recipient mouse with anesthesia machine settings of 2% isoflurane and oxygen flow rate of 2 L/min. Reduce the isoflurane levels to about 1% once the mouse has been anesthetized.

3.3 After the mouse is sedated (confirmed by no-response to toe pinch), clean the outside of the MIW glass with a cotton applicator and glass cleaner, add eye ointment to prevent drying, and insert a tail vein catheter if necessary.

3.4 To maintain proper hydration, give an initial injection of 0.5 mL PBS sub-cutaneously or 100 µL through the tail vein catheter. Repeat every 2 h for the duration of the imaging session.

3.5 Once the mouse has been properly prepared, gently transfer it to the pre-warmed microscope stage.

3.6 Lay the mouse on the microscope stage, fit the isoflurane hose and press the collar of the MIW into a 14 mm receiving hole in the stage insert to stabilize the images. Bring the imaging field into focus using the microscope oculars and bright field illumination observing vasculature with blood flow.

3.7 Check the stability of the field of view. If breathing movement artifacts are present, apply gentle compression to the backside of the gland with a small foam block and a cincture-like piece of adhesive tape. After compression is applied, verify that blood flow is maintained throughout the field of view.

3.8 Periodically adjust the isoflurane levels in 0.25% increments during the imaging session to maintain a proper level of sedation by manually counting animal respiration.

3.9 Maintain a rate of 36–40 respirations per min (rpm) to improve animal longevity and optical imaging. Lower respiration rates can result in the mouse not surviving the experiment, whereas respiration rates over 60 rpm may result in poor sedation, which can increase breathing and motion artifacts in the image data.

4. Set up for 4D, intensity-based, label-free intravital imaging of dynamic cell behavior

4.1 Once the mouse is sedated and securely positioned on the inverted microscope stage, start locating regions of interest. For time-lapse measurements, use a water-based gel instead of water for the objective to reduce evaporation that can lengthen the imaging session. Please see the Table of Materials for details of the optical components.

4.2 Using a light source directed at the MIW, use the oculars of the microscope to identify potential areas for investigation. Add and save the x, y positions in the software to return to these

positions.

NOTE: The fine details of the tumor will not be readily visible with this type of illumination. The goal is simply to identify regions for further investigation. The focus is on seeing vasculature and blood flow.

4.3 After several positions have been saved in the software, preview the chosen fields of view using 890 nm excitation and the FAD/SHG filter cube. Use a maximum dwell time of 4 µs with lower power and high PMT setting. The goal is to preview the fields of view without overexposing the tissue to excessive laser light.

4.4 Once appropriate power levels have been set, set up the z-stacks. Observe appearance of abundant collagen fibers (SHG) at 20–50 µm beneath the glass surface of the MIW. Collagen will become less prevalent as the microscope sections deeper into the tumor (**Figure 1B**). Voids in the SHG reveal the location of tumor masses.

4.5 Set the top z-slice, beneath the layer of solitary cells where the first collagen fibers appear at ~50–100 µm. Set the bottom z-slice at ~250 µm, where the fibers fade out and the poor signal dominates. Repeat this for all x-y positions saved.

4.6 Once the z-stack range is set, increase the dwell time (up to 8 µs) and optimize the power and detector settings. Optimize the power levels needed to excite the tissue for each experiment. Using powers up to 90 mW at 750 nm or 70 mW at 890 nm at the back aperture of the objective are within an acceptable range.

NOTE: The imaging depth, amount of scattering within the tissue, objective characteristics, and detector sensitivity will all significantly impact the amount of power needed to get an image.

4.7 Adjust the time intervals according to experimental goals. Start with 10 min intervals between collection points for most intravital migration movies.

4.8 Even though 2P excitation is gentle on cells and tissues, be cognizant of signs of phototoxicity, like cell blebbing or rapidly increasing autofluorescence, and excessive photobleaching. Reduce laser power or increase timelapse intervals as conditions indicate.

5. Fluorescence lifetime imaging (FLIM) of NAD(P)H

5.1 While preserving the x-y positions from the timelapse acquisitions, set up the microscope to collect a FLIM stack. Insert a 440/80 filter into a filter holder in front of the GaAsP detector, and set the GaAsP detector voltage to 800 in the software. Turn off the room lights when the detectors are on.

5.2 In the software, switch from the galvanometer-based intensity imaging to a FLIM imaging mode.

5.3 For the purpose of identifying and masking the vasculature, set the resolution to 512 x 512 pixels. For collecting complementary metabolic information, set the resolution to 256 x 256 pixels to increase the temporal resolution of the lifetime signature. Set the dwell time to 4 µs and tune the laser to 750 nm.

5.4 Start preview scanning and begin to adjust the laser power. Adjust the laser power until the readout for the constant fraction discriminator (CFD) is between 1 x 10^5 and 1 x 10^6. Do not exceed 1 x 10^6 as this will result in photon pileup and poor overall results.

5.5 Once the power level is set, set the integration time between 90 s and 120 s and start the FLIM collection. It will acquire photons from the field of view for the allotted time.

5.6 Optional: After all necessary collections have been made and the mouse has been removed from the stage, collect an instrument response function (IRF). Measure the IRF by imaging the surface of commercially available urea crystals in a glass-bottom dish with the same parameters and set up used for imaging the tissue.

NOTE: The IRF accounts for any delays or reflections due to the electronic or optical setup. The IRF is convolved in all FLIM acquisitions, and deconvolving it from the data can improve the accuracy of calculated fluorescence decay curves. With that said, the calculated IRFs can often reasonably replicate the quality of the fluorescence decay curves from measured IRF. It is good practice to measure the IRF until it has been determined that the calculated IRF will yield equivalent fits of the decay curves and adequately approximate the results from the measured IRF.

6. Analysis of NADH Lifetime images

6.1 Open FLIM software and import the NAD(P)H lifetime image from the dataset. For more details on how to properly use the software, please consult the fluorescent lifetime handbooks (See Table of Materials).

6.2 To begin, define the model parameters in the software. In the menu bar, click **Options > Model**. Select the following boxes: **Settings** > **Multi-Exponential Decay**, **Fit Method** > **MLE**, **Spatial Binning** > **Square**, **Threshold** > **Peak**, and check **Fix Shift Before Calculating Image.**

6.3 In the menu bar, click **Color > A_1%** from the drop-down menu. On the right side of the window, define it as a three-component fit. Set the **Bin Size > 3.**

6.4 Adjust the **Threshold > ~10**. Re-evaluate threshold accuracy after the decay matrix has been calculated for the first time.

6.5 Fix the τ1 to 200 ps. This represents the short lifetime of red blood cells. Try to find the value that best matches multiple spots in the larger blood vessel, which can be seen in the

intensity image. Fix the τ2 to 1200 ps. This represents the long lifetime of red blood cells.

NOTE: The set values are just the starting point. The values will need to be optimized to bring out the vasculature more. In most cases, but not always, these values will decrease.

6.6 Under **Calculate** in the menu bar, select **Decay Matrix**. This will generate an initial A_1% lifetime images with the vasculature having high values. Use the cursor (crosshairs) to hover over the vasculature. Systematically and one at a time, float (uncheck the **Fix** box) the τ1 and τ2. Record these values as they will help optimize the fixed parameters.

NOTE: The goal is not necessarily to get the most accurate values in the image, but rather to maximize the disparity between the vasculature and tissue without dramatically decreasing the area identified as vasculature.

6.7 Once the appropriate parameters for τ1 and τ2 have been identified, in the menu bar select **Calculate** > **Batch Processing**. Ensure that most settings are similar between z-slices.

6.8 Make sure to verify that there is no one setting grossly different than the others. If so, adjust the shift first and try again. If the issue persists, refit using new parameters. An incorrect shift can be a large cause of noise in the fits and can increase A1% values in the adjacent tumor regions.

6.9 In the menu tab, save the files and then export A_1% files. Upload these files in ImageJ for masking and segmentation.

7. Image segmentation of the vasculature

7.1 Open ImageJ and import the A_1% image as a text image. Repeat this for all images within the stack.

7.2 With all the A_1% images opened, select **Image > Stack > Z-Project**. Use the **Max Intensity Projection** and save the images. See **Supplemental Data 1** for a representative image.

7.3 Go to **Plugins > Segmentation**. Select the trainable **WEKA segmentation plugin**[38].

7.4 Once the WEKA window opens, use the default settings and begin to train the software by creating two classes and tracing lines over the vasculature (high A_1% regions) and non-vasculature (low A_1% regions).

7.5 Continue to add new traces to the two classes until the software consistently identifies the high A_1% regions of the vasculature while eliminating any higher regions of background noise. See **Supplemental Model** for representative classifier model.

7.6 Once the classified image is produced, click on **Image > Type > 8 Bit**. Threshold the image

and create a mask. If the thresholded image still needs to be cleaned up further, use the **Analyze Particles** function.

7.7 Adjust the size and circularity until any smaller and circular regions of the thresholded image are excluded. A clean mask with only the vasculature and very little background is obtained.

7.8 Click on **Edit > Selection > Create Selection.** Transfer the selection to the ROI manager by clicking on **Analyze > Tools > ROI manager**.

7.9 Duplicate the classified image. Proceed to **Process > Binary**. To expand the mask and define the distance from the vasculature that will be included in the image segmentation, select **Dilate**. Repeat until the mask has expanded to the desired range. Record this region of interest (ROI) in the ROI manager.

NOTE: The goal of this step is to quantify the amount or behavior within a certain proximity of the blood vessel (for example, the number of cells present within X µm of the blood vessels). The amount of dilation required is entirely determined by the scientific question.

7.10 To quantify the number of cells within the restrictive regions, select the window (image/channel) of interest. This can be any window that shares the same field of view as the vascular mask. Apply both ROI's using the **XOR** function from the drop-down menu.

NOTE: This operation will measure the items within the desired distance from the vasculature, excluding the vasculature itself. This combined ROI approach can then be used to measure a multitude of parameters, such as intensity, cell number, or migration.

8. Image segmentation of the tumor nest

8.1 Open the NADH image from either a high-resolution intensity scan or FLIM collection in ImageJ.

NOTE: This can be done on individual z-slices, full stacks, or applied to z-projections of a few slices.

8.2 Go to **Plugins > Segmentation**. Select the trainable **WEKA segmentation plugin**.

8.3 Once the WEKA window opens, use the default settings and begin to train the software into two classes of NADH high regions and NADH low regions. The NADH-high regions will have a very discernable pattern of cells with nuclei and the software will easily identify it.

8.4 Continue to toggle back and forth with the overlay to refine the algorithm with additional training until it recognizes all regions of the tumor as determined by eye and prior knowledge of tumor morphology. This is an iterative process.

8.5 Once the algorithm recognizes all the regions of the tumor, select the **Create Result** button. This will produce a new image. Duplicate this image.

8.6 Select the first duplicated image and convert it to an 8 bit image by selecting **Image > Type > 8 Bit**. Threshold this image to create a binary mask. Then create a selection and transfer it to the ROI manager. These ROIs will define the stroma.

8.7 Select the second of the duplicated image and convert it to an 8 bit image. Invert this image by selecting **Image > Edit > Invert**, and then threshold this image to create a binary mask. Once again create a selection and transfer it to the ROI manager. This ROI will define the tumor nest.

9. Image segmentation by fiber organization or alignment

9.1 To begin, open the SHG images, prepare any z-projection, and assess the need for any pre-processing. For good results, high-quality images with discernable fibers and low noise are required.

9.2 Optional: For preprocessing in ImageJ to increase signal-to-noise (SNR) of the SHG channel, subtract the background using a rolling ball subtraction. For most applications, use a rolling ball subtraction between 20 pixels and 50 pixels. Then smoothen the image and save it.

9.3 Open the OrientationJ plugin and set the processing parameters. In the OrientationJ window, define the size of the local tensor window. For a 20x image of this fiber density, set 10 pixels to 15 pixels as a starting point.

9.4 Select **Cubic Spline** as the gradient model and check the **Color Survey Box**. Define the color survey. Set both the **Hue** and **Saturation** as **Coherency**, and then define the **Brightness** as **Original Image,** hit **Run**.

9.5 The output file of the plugin is RGB colormap. Adjust the value of the local tensor window until aligned regions, as determined by the eye, are properly highlighted with blue and magenta hues.

9.6 Once the output image is satisfactory, separate this RGB image into 3 channels. Select I**mage > Color > Split Channel**.

9.7 To enhance the appearance of aligned regions for the purpose of masking, use the image calculator by selecting **Process > Image Calculator**. Using this operator, subtract the green image from the blue image. For a more restrictive mask, subtract the green image from the red image. For random regions, subtract the blue channel from the green channel.

9.8 Threshold the resulting image using the **Moments** algorithm. In most cases, this should

not need further adjustments. However, adjust if needed. This will produce a binary image.

9.9 Once the binary image is made, fill the holes by selecting **Process > Binary > Fill Holes** between fibers and round out the boundaries of the mask using a median filter. A median filter of 10 is a good starting point, adjust it to make a good fit for the data. Manually inspect the mask for agreement and remove any ROIs that are erroneous.

9.10 Once the mask is satisfactory, create a selection by selecting **Edit > Selection > Create Selection**. Transfer this selection to the ROI manager.

REPRESENTATIVE RESULTS:

The installation of the MIW and basic experimental planning are the first steps in this process. This particular MIW design and protocol are more amenable to longitudinal studies[19] and has been successfully utilized with both upright and inverted microscopes. In this case, an inverted microscope was used as it has resulted in greater image stability of the mammary gland with fewer breathing artifacts. In **Figure 1A**, we provide the dimensions of the rigid MIW and a graphical overview of the implantation process.

A typical field of view within a label-free MMTV-PyMT[39] mammary tumor (**Figure 1B–E, Figure 3A**) is very heterogeneous, comprising of collagen fibers, numerous stromal cells, masses of tumor cells, and vasculature (**Figure 3A**). In general, collagen fibers are more abundant near the window and decrease in abundance deeper into the tumor (**Figure 1B–E**) The organization of the fibers surrounding the tumor masses can also be quite varied, often with regions of more random organization in the same field of view as regions of higher alignment (**Figure 2D,H and Figure 3I**).

To develop an analysis pipeline that can segment intravital data into perivascular regions, tumor and stroma, this protocol focused on using the signal from endogenous NAD(P)H and SHG. While identification of the tumor and stroma can be straightforward, the identification of perivascular regions within the tumor microenvironment can be challenging. The vasculature often resides within the narrow ribbons of reduced NAD(P)H signal between the bright NAD(P)H+ cancer cell masses. It is important to note that not all dark boundaries harbor vasculature; rather, some dark regions are simply tumor folds or the butting up of adjacent tumor lobes (yellow arrow, **Figure 2G**). Moreover, while a seasoned eye can extract the bigger diameter blood vessels from the tumor as they have a distinctive appearance, this distinction is not always trivial. This is especially true for smaller diameter vessels where their appearance may be more subtle and variable. In this case, the use of the fluorescence lifetime of NAD(P)H can aid in the positive identification of the vasculature (**Figure 2B,F**). Fluorescence lifetime (FLIM) does not measure the abundance or intensity of photons at a location, but the time it takes for those excited molecules to decay to their ground state. Red blood cells (RBC) and blood plasma have been shown to have a characteristically short and distinctive fluorescence lifetime[32, 37] that can be leveraged for the identification and segmentation of vessels in tissues.

To determine how well the fluorescence lifetime of NAD(P)H identifies the vasculature intravitally, a 100 µL bolus of a rhodamine-labelled dextran was injected into the tail vein after

collecting the FLIM image. Comparisons of maximum intensity projections of NAD(P)H FLIM closely mirror those vessels labeled with a fluorescently labeled dextran (**Figure 2I–J**). Repeating this approach in multiple mice demonstrated that the average mask area from the FLIM image over the area of the dextran mask was 78.6% ± 12.3% (**Figure 2L**). While the overlay was not 100%, this technique was accurately mapping the entire vascular network. The differences observed in the reported areas could often be attributed to intravital drift or registration issues, thinner vessel diameters due to model fitting, or the loss of fine vessels due to RBC exclusion by the pressure of the growing mass. Importantly, this technique works equally well in the presence of both genetically encoded fluorophores like GFP or label-free tumor models (**Figure 2D,H**), thereby providing a very robust and broadly applicable means of identifying the vasculature for image segmentation.

To delineate the boundaries of label-free tumor masses, NAD(P)H autofluorescence (**Figure 1C**) was used. This can be captured by either independently collecting a NAD(P)H image or summating the NAD(P)H FLIM data to generate an intensity image. Either route will allow for suitable segmentation of the tumor microenvironment. As a general observation, two-photon excitation of NAD(P)H in cancer cells elicits bright autofluorescence producing an image that shows crisp individual cells with darkened nuclei (**Figure 2E,G**). This pattern can be used to define the extent of the growing mass. While simple intensity-based thresholding of NAD(P)H is possible to define the boundary of the tumor compartment, a trainable segmentation tool often performs better (**Figure 3B,E**). Some other common readouts, like cell migration or cellular protrusive analysis, may benefit from genetically encoded exogenous fluorescence within the mouse model or the implantation of fluorescently labeled cell lines (**Figure 2A**). In these cases, the task of demarcating the boundary of the mass can be accomplished with simple thresholding of the fluorescent protein. Sometimes the expression of the fluorophore can become quite heterogenous after implantation. This should not cause segmentation problems. Also, it has often been observed that tumors created by fluorescent allografts or xenografts have less compartmentalized regions of collagen fibers than tumors created by genetic tumor models like MMTV-PyMT[40].

The stromal compartment encompasses the regions outside the growing mass or between growing masses, and a mask for the stroma is obtained by inverting the tumor ROI (**Figure 3B-F**). The stromal compartment can then be further compartmentalized into sub-ROIs based on collagen fiber architecture. Collagen fibers are a significant feature in the stroma and have a large diversity of fiber organizations, which are known to modulate cell behavior[41, 42]. Often numerous local (<100 µm) regions of aligned or random fibers exist within the image[40]. Therefore, regions of relatively aligned (red/blue hues) or random (green hues) fiber organization (**Figure 3I**) were identified with the OrientationJ plugin. Using the OrientationJ coherency color map, masks based on the local fiber organization can be created for segmentation purposes (**Figure 3J**). These masks can then be overlaid to analyze differential dynamic stromal cell behavior (**Figure 3K**) due to the effects of specific fiber organization (**Figure 3H,I**).

Now that ROIs for the various compartments of the tumor microenvironment have been defined, they can be applied to the individual frames or channels of the intravital timelapse movie. At this

point, it is important to emphasize that all the signals shown in **Figure 3A** are derived entirely from endogenous sources. This image demonstrates the rich potential of spatial and contextual cues that can come from purely endogenous, ubiquitous, and label-free sources. Here, we used the MMTV-PyMT tumor model as an example to illustrate the applicabilty of the method to quantify the number and characteristics of macrophages within specific locations of the tumor microenvironment (TME). A previous intravital study[43] has shown that cells emitting high levels of FAD autofluorescence (**Figure 3A**, magenta cells, yellow arrows) stain positively with F4/80 antibodies and represent a population of macrophages within the TME. Using this workflow to segment the image, it is possible to efficiently and accurately examine the number, monitor cell-cell interactions over time, or even observe the metabolic characteristics of this subset of macrophages (magenta) within different compartments of the TME (**Figure 3A**, yellow arrows). For example, the behavior of FAD-high macrophages that specifically reside within the NAD(P)H-high tumor nest can be characterized (**Figure 3E**). Similarly, the behaviors of macrophages with respect to the local organization of the fibers in the stroma region can be examined. Some recent reports have indicated that macrophages and other migrating cells in the stroma are responsive to mechanical cues from their local microenvironment[40, 44, 45]. Using the fiber alignment masks produced by this method, it is possible to examine their differential behaviors between regions of random and aligned collagen organizations. Lastly, this same focused analysis can also be applied to determine the number and the behavior of macrophages localized within a defined proximity to the vasculature. In **Figure 3G**, the vasculature can be seen in red, and macrophages can once again be seen in magenta. A mask for the vasculature using NAD(P)H FLIM was created and then expanded through dilation of 10 pixels. The distance chosen was arbitrary for demonstration purposes but can be optimized for the particular needs of the individual experiment. Importantly, while this image is of a single z-slice, this procedure could be easily extrapolated to 3D stacks to observe behavior around the entire volume of the vessel.

FIGURE AND TABLE LEGENDS:

Figure 1: Graphical abstract of mammary window implantation and the underlying organization of an MMTV-PyMT tumor. (**A**) The dimensions of the mammary imaging window and schematic for the general implantation process. (**B–F**) This is a montage from an unlabeled MMTV-PyMT tumor representative starting from 50 µm beneath the surface of the MIW and continuing to a depth of 80 µm. The depth values are provided beneath each image. Collagen fibers (gray) are more prevalent at the surface of the tumor (NAD(P)H, blue) than at greater depths. Scale bar 100 µm.

Figure 2: Representative intravital image of a GFP labeled and label-free PyMT tumor and validation of NAD(P)H FLIM as a marker for the vasculature. A composite image (**A**) of a typical allograft of GFP-4T1 cells into the mammary fat pad and a representative mammary tumor from an MMTV-PyMT tumor model (**E**). NAD(P)H FLIM (**D**) maps the vasculature in both models (**B,F**). GFP fluorescence (**C**) and NAD(P)H autofluorescence (**G**) were used to identify the tumor. Collagen was visualized by SHG (**D,H**). A composite image using NAD(P)H FLIM to identify vasculature was validated by comparing maximum intensity projections of the intravital stack before and after tail vein injection of fluorescent dextran (**I,J,K**). The quantification of four mice

(color identifies individual mice) and fields of view (individual dots in graph) is shown in (**L**). Scale bars 100 µm.

Figure 3: Representative image segmentation using endogenous fluorescence within label-free PyMT tumor. A composite image (**A**) of a single z-slice from a typical mammary tumor was collected using intrinsic signals only. SHG (gray) visualizes the collagen fibers of the tumor. Fluorescence lifetime imaging of NAD(P)H autofluorescence (Tau (τ) mean) reports the metabolic signatures of the cells (green to orange hues) and the location of blood vessels (red). FAD autofluorescence (magenta) identifies macrophages. Using the segmentation scheme outlined in this protocol, the label-free tumor was segmented into compartments for the tumor nest (**B,E**), stroma (**C,F**), and vasculature (**D,G**) using only SHG and NAD(P)H autofluorescence. The stroma and collagen fibers (**H**) can also be classified into local regions of aligned fibers ((shown in magenta/blue), **J,K**). Scale bars 100 µm.

Supplemental Data 1: Representative data set of fitted A_1% from NAD(P)H FLIM. This is a maximum intensity projection of a fitted A1% from a typical data set. It is a representative of the quality of identification possible and a typical level of background before using the trainable classifier.

Supplemental Model: Representative classifier used on fitted A_1% for the identification of the vasculature. This is a sample classifier model for use in the trainable WEKA segmentation plugin within ImageJ.

DISCUSSION:

The 4D intravital imaging is a powerful tool to investigate dynamic physiological interactions within the spatial and temporal context of the native tumor microenvironment. This manuscript provides a very basic and adaptable operational framework to compartmentalize dynamic cell interactions within the tumor mass, the adjacent stroma, or within proximity to the vascular network using only endogenous signals from second harmonic generation or NAD(P)H autofluorescence. This protocol provides a comprehensive, step-by-step method from implantation of the imaging window to image acquisition, analysis, and segmentation. We believe this technique will contribute to a needed analysis framework to segment and quantify 4D intravital data.

This protocol was developed to be broadly compatible with numerous intravital mouse models, including unlabeled PDX models. PDX's are an incredibly informative model[46] but pose a challenge to intravital imaging because the nature of the PDX model is not well-suited for genetic manipulation. Therefore, it would be quite advantageous to be able to visualize dynamic interactions in PDX models within a physiological environment while still being able to segment the images using solely endogenous metabolites like NAD(P)H and second harmonic generation (SHG). In addition to being advantageous for PDX models, this multidimensional approach could be theoretically applied to any tumor or normal tissue study that needs spatial and structural context to address a physiological question. NAD(P)H autofluorescence and SHG from collagen fibers are ubiquitous to all tissues and represent a universal and free resource in intravital

collections. It is also notable that this FLIM approach to identifying the vasculature is robust even in the presence of fluorescence from exogenous sources like GFP. Lastly, SHG and NAD(P)H emission can be visualized in the blue spectrum, thereby residing in a wavelength that is not typically used in the imaging of fluorescent fusion constructs.

The aspect of this approach that is novel and has particular added value is the label-free identification of the vasculature. While other approaches can work, the use of the fluorescence lifetime of NAD(P)H easily provides a clear signature without additional labeling. The data shows that the lifetime-defined vessels mirror the vasculature labeled from tail vein injection of fluorescent dextran, the gold standard for vasculature imaging. Our technique excels at visualizing smaller blood vessels compared to simple two-photon or three-photon excitation, where larger vessels are easily visualized, but smaller ones require more expertise to identify. The lifetime signature is unambiguous for all vessels, regardless of size. Moreover, this additional NAD(P)H FLIM acquisition can be easily combined with other markers for the segmentation of the tumor microenvironment. Through a single FLIM acquisition of NAD(P)H, the requirements for defining the vasculature, tumor nest, and stroma are achievable. The FLIM collection can be incorporated into the existing experimental design by collecting a single acquisition at the end or beginning of a time series or interleaving the collections throughout the entire 4D acquisition. Determination of the appropriate amount of FLIM images will depend on specific experimental needs and constraints, like acquisition intervals, experimental duration, or image stability, but at a minimum, one FLIM collection per 4D series will be needed for this method.

This process of utilizing NAD(P)H FLIM for the identification of the vasculature requires mathematically fitting the FLIM data to an exponential function of the form

$$f(t) = A_1 e^{-t/(\tau 1)} + A_2 e^{-t/(\tau 2)} + A_3 e^{-t/(\tau 3)}$$

with $A_1+A_2+A_3=1$. While most lifetime images of NAD(P)H reported in the literature are fitted as a bi-exponential, in this application NAD(P)H was fitted as a tri-exponential where the τ1 and τ2 are set to the reported values of RBC's and τ3 is allowed to float. Importantly, the goal is not to achieve the most accurate lifetime value, but rather to provide an optimal image for segmentation. When the τ1 and τ2 values are initially fixed at the reported values of RBC's[32, 47] and the matrix is calculated, the blood vessels will stand out with A_1% values greater than 60% in the blood vessels and A_1% values generally less than 40% in the adjacent tumor. The next step is to try to maximize the A_1% in the blood vessels while minimizing the A_1% in the adjacent tumor. This is an iterative process, and by the end of it, the A_1% values of the blood vessels will be greater than 90% with the A_1% values of the tumor less than 10%. Once the A_1% values of the blood vessels are uniformly high and the background is uniformly low, export these A_1% files into a trainable segmentation tool. This will quickly remove any remaining noise and define the ROI for the vasculature.

As the mammary fat pad is located outside of the body cavity, the surgery is minimally invasive, and the best results are obtained by implanting the MIW over the 4th inguinal mammary gland. The timing of window implantation and when the experiment will be conducted is critical. It is best to allow for 24 – 48 h of healing post-surgery before the physiological timepoint that will be investigated. While the procedure itself only requires a small incision (≈ 10 mm) to insert the

window (**Figure 1A**), post-surgery healing time will permit any inflammation and fluids that accumulated due to the implantation process to clear. Moreover, it will also allow the tumor to continue to grow into the window. Both factors will improve the overall image quality by decreasing opacity/scattering and increasing image stability. The next thing to consider is the planned total duration of the experiment. While these windows were designed for longitudinal studies, the rigid nature of the window incurs a time limit of 2 to 3 weeks. After that timespan, the window has a tendency to dislodge from the dermal layer, thereby contaminating and terminating the experiment. If a longitudinal study of the mammary gland is not required, other intravital methods like a terminal skin flap procedure[22] that eliminates the surgical implantation of a MIW may be a better option. The skin flap procedure provides better access to the entire gland as it is not constrained by the placement and dimensions of the MIW, and it can produce greater image stability as the gland is pulled away from the body cavity. Regardless of the intravital imaging approach, the segmentation of the microenvironment using endogenous fluorescence is still broadly applicable for subsequent image analysis. The last thing to consider is the duration of the individual imaging experiment. It is not unreasonable to acquire movies lasting 6–8 h. However, during the longer collections, hydration becomes an issue, and close monitoring of the health of the mouse is required.

One significant advantage of this method is that the various images of endogenous fluorescence required for segmentation of the tumor microenvironment can be collected with relative ease and without additional manipulations to the mouse. With the filter/dichroic combination reported here (Table of Materials), both SHG and NADH images can be acquired with the same filter set by switching wavelengths from 890 nm to 750 nm. While this creates an acquisition delay, it does not impact subsequent image segmentation. It is also important to remember that this method represents a mere starting point for a segmentation technique using endogenous fluorescence, and more advanced optical configurations may allow for simultaneous acquisitions if needed.

There are limitations of using FLIM to identify the vasculature. The FLIM approach requires specialized electronics, instrumentation, and expertise to collect. However, all these requirements are increasingly more integrated into modern microscopes and more available through the use of imaging core facilities. FLIM has become a mature technology and acquiring good data does not require much training. A second limitation is that FLIM acquisitions are time-consuming. While the frame rate for an image collected with fluorescent dextran is about a second or less, the average FLIM collection can range from 60 s to 120 s, which may be prohibitive if the physiological timepoints are shorter than that. FLIM identification of the vasculature is not intended to replace all tail vein injected fluorescent dextran or multiphoton excitation of the vasculature; rather, it is yet another approach in the growing toolbox for intravital imaging. Furthermore, we anticipate that longer acquisition times will be made dramatically shorter in the coming years. The detectors and electronics are rapidly improving, decreasing the detector dead time, and thereby requiring shorter acquisition periods to capture the same number of photons. The second reason to be optimistic of shorter acquisition times is the emergence of machine learning software or image restoration algorithm like CSBDeep[48]. These algorithms could be potentially trained to work with shorter exposure times and reduce the number of photons

needed to accurately identify structures for segmentation purposes. Together, this could rapidly reduce the timeframes needed for these multidimensional acquisitions.

The use of intravital imaging will only become more important as researchers try to unravel the many complex cell-cell and cell-matrix interactions that occur within the physiological tumor microenvironment. Therefore, continued developments in the acquisition, segmentation and analysis capabilities are needed. Towards this end, it is important to not overlook the potential of endogenous fluorescence images for microenvironment segmentation. In this protocol, the endogenous signal from SHG and fluorescence metabolites, including NAD(P)H intensity and FLIM, was used for segmentation purposes during intravital imaging of the mammary TME. Other endogenous metabolites or intrinsic properties can provide additional signals to reveal the dynamic reciprocity of tumor cells and the microenvironment. For example, FAD can be used to monitor the movement of immune populations[43], 3P generation can highlight structural features like plasma membranes or adipose[36], and elastin fluorescence can be used to separate arteries from veins[47]. Therefore, endogenous fluorescence will continue to provide a rich multi-dimensional platform that should be utilized to the fullest as the research community continues to build the toolbox for intravital microenvironment segmentation and analysis.

ACKNOWLEDGMENTS:

The authors would like to acknowledge NCI R01 CA216248, CA206458, and CA179556 grants for funding this work. We would also like to acknowledge Dr. Kevin Eliceiri and his imaging group for their technical expertise in the early development of our intravital program. We also thank Dr. Ben Cox and other members of the Eliceiri Fabrication Group at the Morgridge Institute for Research for their essential technical design during the early phases of the MIW. Dr. Ellen Dobson assisted with useful conversations about the ImageJ trainable WEKA segmentation tool. In addition, we would like to thank Dr. Melissa Skala and Dr. Alexa Barres-Heaton for the timely use of their microscope. Lastly, we would like to thank Dr. Brigitte Raabe, D.V.M, for all the thoughtful discussions and advice on our mouse handling and care.

DISCLOSURES:

The authors have no conflicts of interest to disclose.

REFERENCES:

1. Eble, J.A., Niland, S. The extracellular matrix in tumor progression and metastasis. *Clinical & Experimental Metastasis*. **36** (3), 171–198 (2019).
2. Afik, R. et al. Tumor macrophages are pivotal constructors of tumor collagenous matrix. *The Journal of Experimental Medicine*. **213** (11), 2315–2331 (2016).
3. Varol, C., Sagi, I. Phagocyte-extracellular matrix crosstalk empowers tumor development and dissemination. *The FEBS Journal*. **285** (4), 734–751 (2018).
4. Winkler, J., Abisoye-Ogunniyan, A., Metcalf, K.J., Werb, Z. Concepts of extracellular matrix remodelling in tumour progression and metastasis. *Nature Communications*. **11** (1), 5120 (2020).
5. Han, W. et al. Oriented collagen fibers direct tumor cell intravasation. *Proceedings of the National Academy of Sciences of the United States of America*. **113** (40), 11208–11213 (2016).
6. Malandrino, A., Mak, M., Kamm, R.D., Moeendarbary, E. Complex mechanics of the

heterogeneous extracellular matrix in cancer. *Extreme Mechanics Letters*. **21**, 25–34 (2018).
7. Lugo-Cintrón, K.M. et al. Breast Fibroblasts and ECM Components Modulate Breast Cancer Cell Migration Through the Secretion of MMPs in a 3D Microfluidic Co-Culture Model. *Cancers*. **12** (5), 1173 (2020).
8. Wozniak, M.A., Desai, R., Solski, P.A., Der, C.J., Keely, P.J. ROCK-generated contractility regulates breast epithelial cell differentiation in response to the physical properties of a three-dimensional collagen matrix. *The Journal of Cell Biology*. **163** (3), 583–595 (2003).
9. Zhang, K. et al. The collagen receptor discoidin domain receptor 2 stabilizes SNAIL1 to facilitate breast cancer metastasis. *Nature Cell Biology*. **15** (6), 677–687 (2013).
10. Malik, G. et al. Plasma fibronectin promotes lung metastasis by contributions to fibrin clots and tumor cell invasion. *Cancer Research*. **70** (11), 4327–4334 (2010).
11. Bae, Y.K., Choi, J.E., Kang, S.H., Lee, S.J. Epithelial-mesenchymal transition phenotype is associated with clinicopathological factors that indicate aggressive biological behavior and poor clinical outcomes in invasive breast cancer. *Journal of Breast Cancer*. **18** (3), 256–263 (2015).
12. Wei, S.C. et al. Matrix stiffness drives epithelial-mesenchymal transition and tumour metastasis through a TWIST1-G3BP2 mechanotransduction pathway. *Nature Cell Biology*. **17** (5), 678–688 (2015).
13. Riching, K.M. et al. 3D collagen alignment limits protrusions to enhance breast cancer cell persistence. *Biophysical Journal*. **107** (11), 2546–2558 (2014).
14. Carey, S.P. et al. Local extracellular matrix alignment directs cellular protrusion dynamics and migration through Rac1 and FAK. *Integrative Biology: Quantitative Biosciences from Nano to Macro*. **8** (8), 821–835 (2016).
15. Ray, A., Morford, R.K., Ghaderi, N., Odde, D.J., Provenzano, P.P. Dynamics of 3D carcinoma cell invasion into aligned collagen. *Integrative Biology: Quantitative Biosciences from Nano to Macro*. **10** (2), 100–112 (2018).
16. Szulczewski, J.M. et al. Directional cues in the tumor microenvironment due to cell contraction against aligned collagen fibers. *Acta Biomaterialia*. **129**, 96–109 (2021).
17. Esbona, K. et al. The Presence of Cyclooxygenase 2, Tumor-Associated Macrophages, and Collagen Alignment as Prognostic Markers for Invasive Breast Carcinoma Patients. *The American Journal of Pathology*. **188** (3), 559–573 (2018).
18. Entenberg, D. et al. A permanent window for the murine lung enables high-resolution imaging of cancer metastasis. *Nature Methods*. **15** (1), 73–80 (2018).
19. Kedrin, D. et al. Intravital imaging of metastatic behavior through a mammary imaging window. *Nature Methods*. **5** (12), 1019–1021 (2008).
20. Jacquemin, G. et al. Longitudinal high-resolution imaging through a flexible intravital imaging window. *Science Advances*. **7** (25), eabg7663 (2021).
21. Boone, P.G. et al. A cancer rainbow mouse for visualizing the functional genomics of oncogenic clonal expansion. *Nature Communications*. **10** (1), 5490 (2019).
22. Dawson, C.A., Mueller, S.N., Lindeman, G.J., Rios, A.C., Visvader, J.E. Intravital microscopy of dynamic single-cell behavior in mouse mammary tissue. *Nature Protocols*. **16** (4), 1907–1935 (2021).
23. Leung, E. et al. Blood vessel endothelium-directed tumor cell streaming in breast tumors requires the HGF/C-Met signaling pathway. *Oncogene*. **36** (19), 2680–2692 (2017).
24. Jain, R.K. Normalizing tumor microenvironment to treat cancer: Bench to bedside to

836 biomarkers. *Journal of Clinical Oncology: Official Journal of The American Society of Clinical*
837 *Oncology*. **31** (17), 2205–2218 (2013).
838 25. Wyckoff, J.B. et al. Direct visualization of macrophage-assisted tumor cell intravasation in
839 mammary tumors. *Cancer Research*. **67** (6), 2649–2656 (2007).
840 26. Baklaushev, V.P. et al. Modeling and integral X-ray, optical, and MRI visualization of
841 multiorgan metastases of orthotopic 4T1 breast carcinoma in BALB/c Mice. *Bulletin of*
842 *Experimental Biology and Medicine*. **158** (4), 581–588 (2015).
843 27. Baklaushev, V.P. et al. Luciferase Expression Allows Bioluminescence Imaging But Imposes
844 Limitations on the Orthotopic Mouse (4T1) Model of Breast Cancer. *Scientific Reports*. **7** (1), 7715
845 (2017).
846 28. Campagnola, P.J., Loew, L.M. Second-harmonic imaging microscopy for visualizing
847 biomolecular arrays in cells, tissues and organisms. *Nature Biotechnology*. **21** (11), 1356–1360,
848 (2003).
849 29. Bredfeldt, J.S. et al. Computational segmentation of collagen fibers from second-harmonic
850 generation images of breast cancer. *Journal of Biomedical Optics*. **19** (1), 16007 (2014).
851 30. Liu, Y. et al. Fibrillar Collagen Quantification With Curvelet Transform Based Computational
852 Methods. *Frontiers in Bioengineering and Biotechnology*. **8**, 198 (2020).
853 31. Püspöki, Z., Storath, M., Sage, D., Unser, M. Transforms and Operators for Directional
854 Bioimage Analysis: A Survey. *Advances in Anatomy, Embryology, and Cell Biology*. **219**, 69–93,
855 (2016).
856 32. Saytashev, I. et al. Multiphoton excited hemoglobin fluorescence and third harmonic
857 generation for non-invasive microscopy of stored blood. *Biomedical Optics Express*. **7** (9), 3449–
858 3460 (2016).
859 33. Harney, A.S. et al. Real-Time Imaging Reveals Local, Transient Vascular Permeability, and
860 Tumor Cell Intravasation Stimulated by TIE2hi Macrophage–Derived VEGFA. *Cancer Discovery*. **5**
861 (9), 932–943 (2015).
862 34. von Au, A. et al. Circulating fibronectin controls tumor growth. *Neoplasia (New York, N.Y.)*. **15**
863 (8), 925–938 (2013).
864 35. Murgai, M. et al. KLF4-dependent perivascular cell plasticity mediates pre-metastatic niche
865 formation and metastasis. *Nature Medicine*. **23** (10), 1176–1190 (2017).
866 36. You, S. et al. Intravital imaging by simultaneous label-free autofluorescence-multiharmonic
867 microscopy. *Nature Communications*. **9** (1), 2125 (2018).
868 37. Yakimov, B.P. et al. Label-free characterization of white blood cells using fluorescence lifetime
869 imaging and flow-cytometry: molecular heterogeneity and erythrophagocytosis [Invited].
870 *Biomedical Optics Express*. **10** (8), 4220–4236 (2019).
871 38. Arganda-Carreras, I. et al. Trainable Weka Segmentation: a machine learning tool for
872 microscopy pixel classification. *Bioinformatics (Oxford, England)*. **33** (15), 2424–2426 (2017).
873 39. Guy, C.T., Cardiff, R.D., Muller, W.J. Induction of mammary tumors by expression of
874 polyomavirus middle T oncogene: a transgenic mouse model for metastatic disease. *Molecular*
875 *and Cellular Biology*. **12** (3), 954–961 (1992).
876 40. Szulczewski, J.M. et al. Directional cues in the tumor microenvironment due to cell
877 contraction against aligned collagen fibers. *Acta Biomaterialia*. **129**, 96–109 (2021).
878 41. Provenzano, P.P. et al. Collagen reorganization at the tumor-stromal interface facilitates local
879 invasion. *BMC Medicine*. **4** (1), 38 (2006).

42. Conklin, M.W. et al. Aligned collagen is a prognostic signature for survival in human breast carcinoma. *The American Journal of Pathology*. **178** (3), 1221–1232 (2011).
43. Szulczewski, J.M. et al. In Vivo Visualization of Stromal Macrophages via label-free FLIM-based metabolite imaging. *Scientific Reports*. **6**, 25086 (2016).
44. Hoffmann, E.J., Ponik, S.M. Biomechanical Contributions to Macrophage Activation in the Tumor Microenvironment. *Frontiers in Oncology*. **10**, 787 (2020).
45. Pakshir, P. et al. Dynamic fibroblast contractions attract remote macrophages in fibrillar collagen matrix. *Nature Communications*. **10** (1), 1850 (2019).
46. Dobrolecki, L.E. et al. Patient-derived xenograft (PDX) models in basic and translational breast cancer research. *Cancer and Metastasis Reviews*. **35** (4), 547–573 (2016).
47. Shirshin, E.A. et al. Two-photon autofluorescence lifetime imaging of human skin papillary dermis in vivo: assessment of blood capillaries and structural proteins localization. *Scientific Reports*. **7** (1), 1171 (2017).
48. Weigert, M. et al. Content-aware image restoration: pushing the limits of fluorescence microscopy. *Nature Methods*. **15** (12), 1090–1097 (2018).

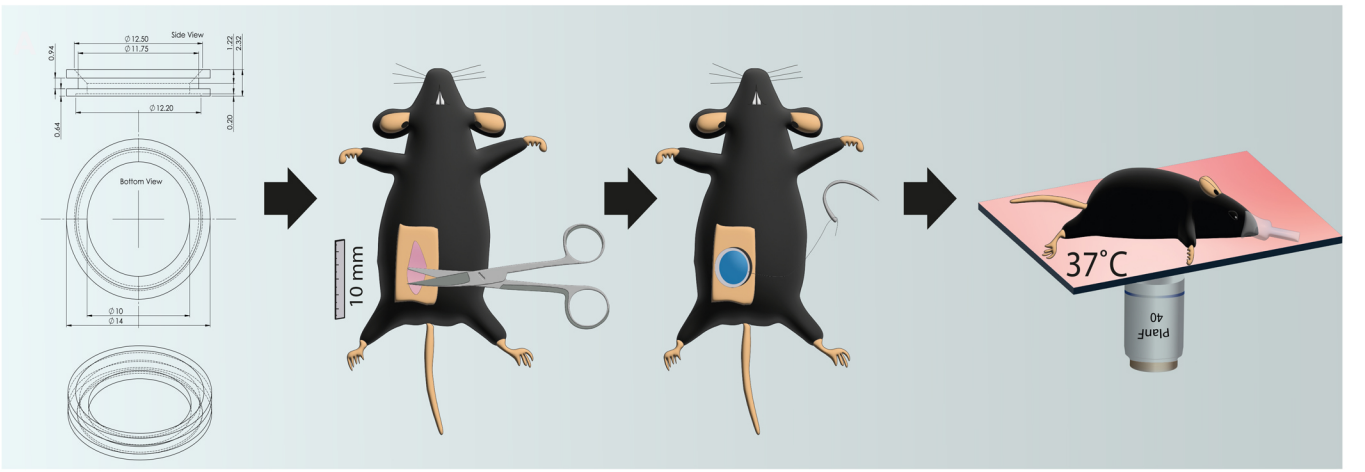

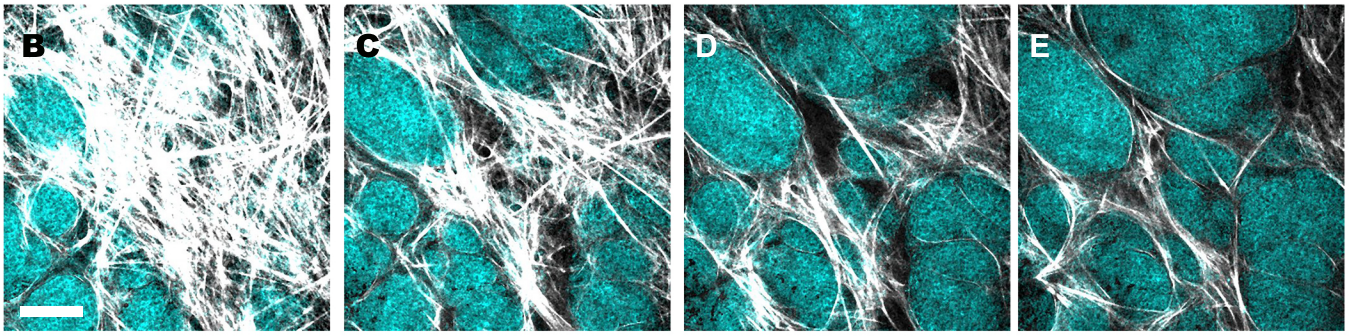

-50 μM -60 μM -70 μM -80 μM

Figure 2

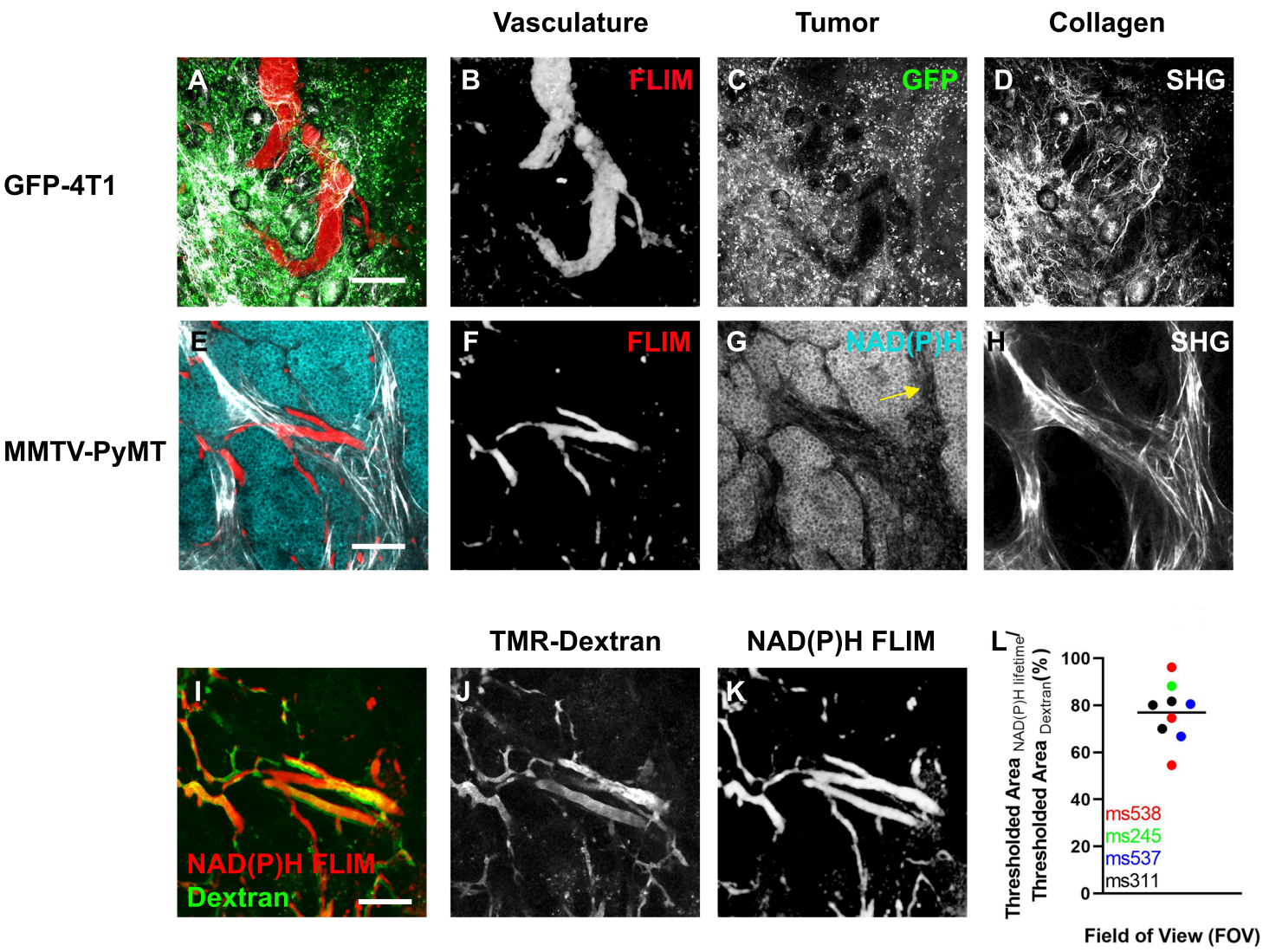

Figure 3

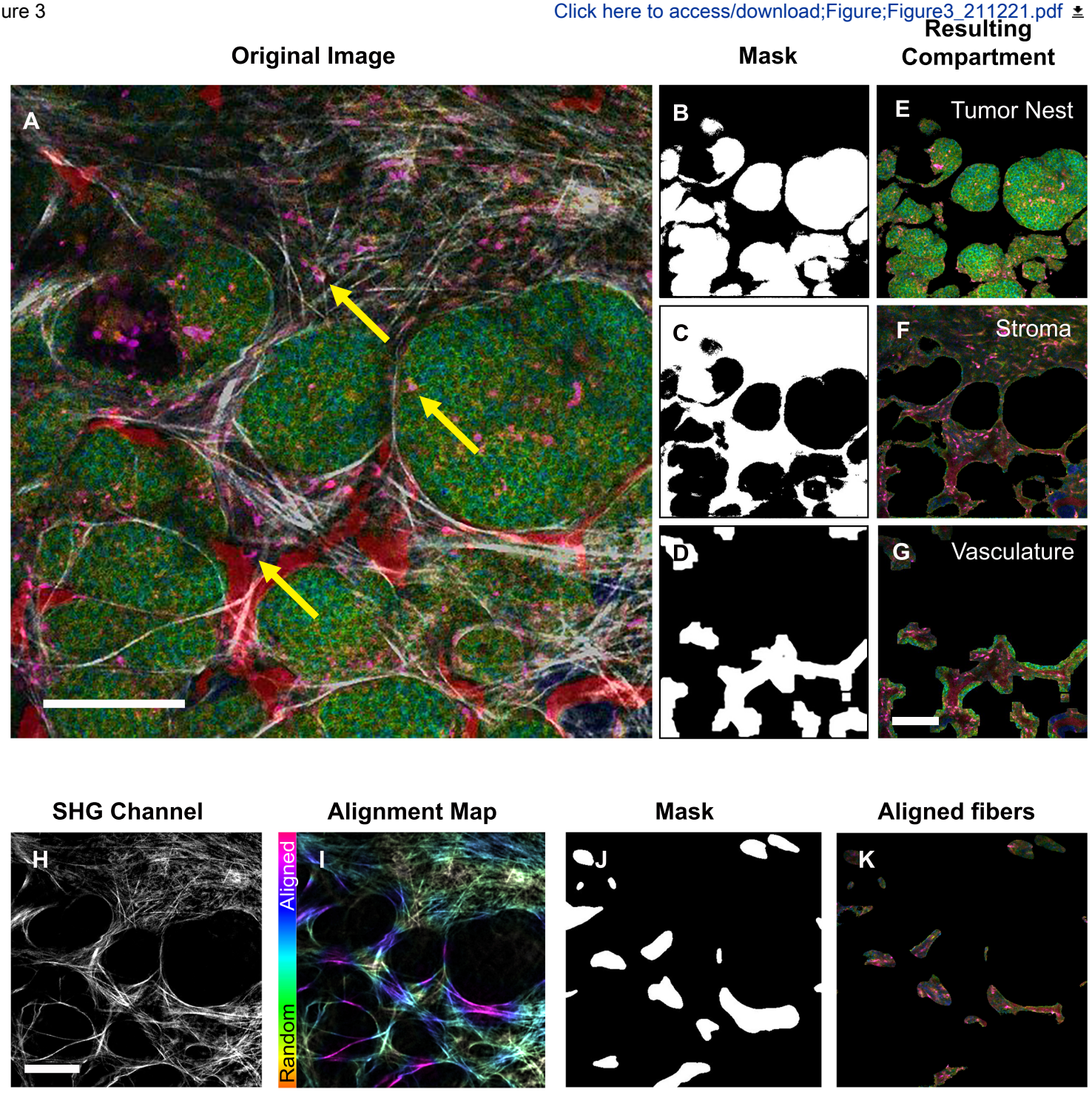

Table of materials

Click here to access/download

Table of Materials

JoVE_Materials_Burkel et al_220104_RE.xlsx

Please note that the reviewers raised some significant concerns regarding your method and your manuscript. Please revise the manuscript to thoroughly address these concerns. Additionally, please describe the changes that have been made or provide explanations if the comment is not addressed in a rebuttal letter. We may send the revised manuscript and the rebuttal letter back to peer review.

Editorial comments:

Editorial changes to be made by Authors:

1. Please take this opportunity to thoroughly proofread the manuscript to ensure that there are no spelling or grammar issues.

2. Please revise the text to avoid the use of any personal pronouns (e.g., "we", "you", "our" etc.). We have removed versions of "we", "you", or "our" from the manuscript

3. Please ensure that the Introduction also includes all of the following:

a) A description of the context of the technique in the wider body of literature

We have added additional lines of text to further describe the technique and why this technique is needed. (lines 86-104 and lines 126-130)

b) Information to help readers to determine whether the method is appropriate for their application

We have added additional lines of text to specify that this method was specifically written for longitudinal intravital imaging of the mammary tumor microenvironment (lines 126-130). However, we also indicate that this would be of value for anyone trying to segment images from intravital movies. I think this technique is broadly applicable.

4. JoVE cannot publish manuscripts containing commercial language. This includes trademark symbols (™), registered symbols (®), and company names before an instrument or reagent. Please remove all commercial language from your manuscript and use generic terms instead. All commercial products should be sufficiently referenced in the Table of Materials (For example: Swift Manufacturing, Warner Instruments, Loctite 1365882, Tokai Hit, Bruker, Coherent Chameleon, PrairieView, Becker and Hickl SPC-150, Hamamatsu H7422P-40, SpcImage, etc.)

All commercial language has been removed and placed into the required Table of Materials excel sheet.

5. Replace ml with mL and µl with µL. Use min for minutes, h for hours throughout the manuscript.

All inappropriate abbreviations have been changed throughout the document.

6. Line 321: please move the website to Table of Materials and refer to it wherever needed.

The website has been moved to the table of materials

7. Please ensure that all text in the protocol section is written in the imperative tense as if telling someone how to do the technique (e.g., "Do this," "Ensure that," etc.). The actions should be described in the imperative tense in complete sentences wherever possible. Avoid usage of phrases such as "could be," "should be," and "would be" throughout the Protocol. Any text that cannot be written in the imperative tense (instructions, remarks, extraneous/cautionary details) may be added as a "Note." However, notes should be concise and used sparingly. Please include all safety procedures and use of hoods, etc.

The paper has been proofread and changed to the imperative tense whenever possible. Statements that are not suitable for the imperative tense were changed to "Notes". There are no additional safety precautions beyond the PPE that is listed that is required.

8. Please simplify the Protocol so that individual steps contain only 2-3 actions per step and a maximum of 4 sentences per step.

We limited our sentences in our protocol to a maximum of 4 sentences per step.

9. The Protocol should contain only action items that direct the reader to do something. Please move the discussion (for e.g., in steps 4 and 5) about the protocol to the Discussion.

All non-actionable language was removed between the sections of the protocol.

10. Please use a single line spacing between steps and substeps of the protocol. Please limit the highlighting to up to 3 pages of the Protocol (including headings and spacing) that identifies the essential steps of the protocol for the video, i.e., the steps that should be visualized to tell the most cohesive story of the Protocol. Remember that non-highlighted Protocol steps will remain in the manuscript, and therefore will still be available to the reader.

Single line spacing was used between all steps and substeps of the protocol, and the highlighted text is limited to 3 pages.

11. Figure 1 and 2: Please include scale bars in all the figure panels.

Scale Bars have been included in all figure panels.

12. As we are a methods journal, please ensure that the Discussion explicitly also covers the following in detail in 3-6 paragraphs with citations:
a) Critical steps within the protocol
b) Any modifications and troubleshooting of the technique
c) The significance with respect to existing methods
d) Any future applications of the technique

The discussion has been modified to include points a – d.

13. Please expand the journal names in references.

We corrected the reference style and now journal names are expanded in the references.

14. Please ensure that all materials/reagents/equipment/software used in the study are listed in Table of Materials along with the associated catalogue and vendor information.

We have verified that the Table of Materials is accurate and includes catalogue and vendor information.

Reviewers' comments:

We thank the reviewers for their helpful comments, which have greatly improved our intravital segmentation protocol. Our point-by-point response to individual comments can be found below.

Reviewer #1:
Manuscript Summary:
The goal of the manuscript is to provide methodology for intravital imaging of the tumor microenvironment, more specifically the interactions between cells and the extracellular matrix (ECM). The authors have described how to achieve these observations without exogenously administered dyes by exploiting collagen second harmonic signal, endogenous fluorescence of NAD(P)H and fluorescence lifetime imaging microscopy (FLIM). As a model

system, MMTV-PyMT mice were utilized, which spontaneously generate mammary tumors and go through similar stages to human breast cancer progression from benign to malignant primary lesions to metastases. The manuscript is very interesting and will be valuable for other imaging researchers. The following major and minor points are recommended to improve the manuscript:

Major Concerns:
* In the discussion of 3D in vitro culture systems in the Introduction, it would also be important to briefly discuss the role of microfluidic tumor models for visualizing cell-matrix interactions and cite a few papers.

While we recognize the importance of microfluidic models to the field, we feel that this is outside of the focus of this protocol. However, to provide our readers with a broad perspective, we have included a brief discussion of microfluidic tumor models and their citations into the first paragraph of the introduction (lines 60-64).

* Limitations of surgical damage in implantation of the window and the inability to capture the whole tumor depth should be noted (specifically how much depth penetration one can achieve with each imaging technique proposed).

We agree with the reviewer, Mammary Imaging Windows (MIW) are not always the best choice for every intravital application. Our surgical methods are based on prior work developed by our collaborators, which aim to minimize tissue damage during surgical implantation of the window (DOI: 10.1038/nmeth.1269). Here, we specified the use of MIWs based on their utility for longitudinal studies and pointed out that terminal skin flap models might be better when more access is needed (lines 459-468). In addition, we reworked figure 1 to include a montage of the tumor taken at different depths.

* The authors could mention that a limitation of conventionally used dyes such as luciferase and green/red fluorescent protein (GFP/RFP) is that they are foreign to the mouse. GFP/RFP and/or luciferase tagged tumor cells that are injected into an immunocompetent mouse will experience a decrease in metastasis compared to these cells injected into immunocompromised mice due to the body's immune reaction against the foreign proteins. You could cite these papers:
o Baklaushev, V. P., Kilpelainen, A., Petkov, S., Abakumov, M. A., Grinenko, N. F., Yusubalieva, G. M., Latanova, A. A., Gubskiy, I. L., Zabozlaev, F. G., Starodubova, E. S., Abakumova, T. O., Isaguliants, M. G. & Chekhonin, V. P. Luciferase Expression Allows Bioluminescence Imaging But Imposes Limitations on the Orthotopic Mouse (4T1) Model of Breast Cancer. Scientific reports 7, 7715, doi:10.1038/s41598-017-07851-z (2017).

o Baklaushev, V. P., Grinenko, N. F., Yusubalieva, G. M., Abakumov, M. A., Gubskii, I. L., Cherepanov, S. A., Kashparov, I. A., Burenkov, M. S., Rabinovich, E. Z., Ivanova, N. V., Antonova, O. M. & Chekhonin, V. P. Modeling and integral X-ray, optical, and MRI visualization of multiorgan metastases of orthotopic 4T1 breast carcinoma in BALB/c mice. Bulletin of experimental biology and medicine 158, 581-588, doi:10.1007/s10517-015-2810-3 (2015).

We agree with the reviewer that this is a limitation of the field. We have now included a new paragraph in the introduction that highlights this point (Lines 94-102), and further demonstrates the need for new segmentation approaches for intravital imaging.

* Is the purpose of this protocol to have other investigators use their own imaging windows for the same procedure or introduce other people in the field on how to perform these techniques? It may be useful to provide a CAD drawing for the mammary ring window or provide a citation for another available drawing so researchers can be pointed to another resource.

To clarify, the purpose of this protocol is two-fold. First, it is meant to show investigators how to install MIW for longitudinal intravital imaging. We have included references and a CAD drawing of the MIW and a cartoon schematic of surgical implantation in Figure 1. The second important purpose of this protocol is the use multi-dimensional endogenous fluorescence that is ubiquitous to enhance the quantification potential of intravital data. The protocol outlines how to collect ancillary images of endogenous fluorescence for the purpose of segmenting the tumor landscape. The benefits of this approach include its flexibility and versatility. It is not dependent on a particular window and in fact we reference other window options in the introduction (line 72-75).

* If bleeding occurs during surgical implantation of the MIW, what is the course of action? How does one avoid bleeding? Are there any special steps to be taken?

Bleeding can occur during this protocol and we supplied a note on how to address it in section 2.6 (Lines 181-184).

* Several items should be added to the material/equipment sheet at the end of the document - forceps, surgical micro-scissors, heating blanket/heating chamber (if what you use is a custom part - please provide other options that can be used instead of this like heating pads, etc), objective heater, custom fitted stage insert (any information that could be provided for this?), Hamamatsu H7422P-40 GaAsP detector, a Becker and Hickl SPC-150 photon counting board.

The table of materials has been updated to give a comprehensive list of the supplies and equipment needed to complete this approach.

* In step 4 "Setup for 4D,..." please be sure to note the configuration of the microscope if it is upright or inverted. Also, details on the objective magnification, NA, and immersion medium is crucial. If it is water immersion, adding water to the mammary window will be important to add. A baseline level of laser power should be specified to start from which would be helpful to avoid tissue damage/photobleaching. It would be helpful to explain what saturation of the detectors means - how can you tell if saturation is achieved? The signs of phototoxicity and photobleaching should be explained.

A note/tip for the use of immersion media was added and a few symptoms of photobleaching and phototoxicity were described. We choose not to elaborate on the PMT saturation because basic microscopy knowledge is a requirement for such an advanced microscopy technique. Therefore, we felt that explanation would be unnecessary and redundant for our readers. Instead, the goal of determining optimal settings has been clarified in the text.

* In Step 5 "FLIM of NAD(P)H...", the setup of the urea crystals should be explained in a little more detail - how are the crystals prepared? Are they dry or in a solution? Which solution? Do they have to be imaged underneath a glass coverslip?

The urea crystals are not prepared; they are commercially available and purchased from a company. The company name and product number were listed in the table of materials. Additional text was added (lines 305-308) to further clarify how the crystals were imaged to collect an instrument response function.

* In Step 7.5 "Image segmentation of the vasculature..." what is the desired result of the thresholded images you are trying to achieve? This could be helpful to write a sentence or two about desired results. In Step 7.8 in the same section, how much dilation is needed? An explanation of the goal of this step would be helpful to better define what is to be achieved.

We thank the reviewer for pointing out the need for clarification in this section. The intent of vasculature segmentation and dilation of the subsequent vascular mask was to demonstrate the possibility of analyzing cells localized at varying distances away from vasculature. The amount of vascular dilation is a parameter that is set by the experimentalist and dependent on the goals of the individual study. An additional note was added to highlight the goal of the dilation (line 369-372).

* In Step 8.3 "Image segmentation of the tumor nest..." What indicates a suitable classifier? This should be specified.

Additional text has been added to better explain the end goal of the segmentation procedure and what is a suitable classifier.

Minor Concerns:
* Representative Results: yellow arrows are mentioned on Fig 1C but there are no yellow arrows in the figure. Please add the arrows.

We apologize for this omission; we have corrected the figure to include yellow arrows.

* Figure 1 caption: it mentions gold stars and red triangles but these shapes are not shown in the figure. Please add them to the figure. The gold stars and red triangles have been removed and eliminated from the captions.

* In Figure 2, the contrast between the red color and magenta colors is not easily discriminated. Picking a different color for either red or magenta in the figure would be helpful.

We agree with the reviewer, the colors and layout of the figure made it difficult to follow. We increased the contrast of the red channel to make the vasculature more obvious. We also added arrowheads to train the readers eye to the magenta-colored macrophages. In addition, the layout of the figure has been modified to better convey the process and possibilities of image segmentation based on endogenous, label-free fluorescence.

Reviewer #2:
Manuscript Summary:
In this useful protocol, Ponik et al. present a full-pipeline to recover stroma structural information from auto-fluorescence (classic, second harmonic generation, FLIM) in intravital microscopy. The authors use this technique to incorporate the stroma dimension to intravital study notably to analyse the stroma resident cells and the overall mechanical backbone of the tissue through isotropic collagen fibres.
This technique is valuable for the field and deserve to be shared. Indeed, intravital microscopy is often half-blind technique and any new imaging dimension allowing structural or positional reference as like any extra information layer is needed. Moreover, FLIM technology is not widely used due to required specialist equipment: inexperienced

users will likely find this work useful and may justify integration of such modules on intravital setups.
However, the manuscript need refinement to be more general and reach a broader audience. Indeed, the technique is not only useful for PyMT stroma study, which is the felt by reading the manuscript and should be opened for use in other conditions (eg. tissue physiology). A review of the animal parts by a vet is strongly recommended. As very practical journal, many "custom" elements must be shared or obtainable. Only based on the manuscript, it is sometime very difficult to visualize.
This protocol will be useful for many once following points will be addressed.

Major Concerns:
- Some important missing information about animal ethics are missing (><) and should be added/modified for worldwide audience (where the ethic become stricter and stricter). A review of this part by the authors' responsible vet could be a good idea before making a movie.

Additional language was added to address the ethical care of the animal and a veterinarian has reviewed the manuscript to verify compliance with our UW-IACUC approved animal protocol (lines 141-144). We also commented on the use of the analgesia/anesthesia and the incision/implantation procedure (lines 170-172).

* 2.0: it may be obvious for authors but an extra bullet point precising that the tools were autoclaving etc... could be a plus.

We agree with the reviewer that a reminder to autoclave materials may be helpful for readers. An extra bullet point was added for autoclaving (lines161-162).

* 2.1: add warming blanket temperature and reference. Precise that auxiliary lighting should be "cold-light" to avoid tissue drying and add a reference. Precise that surgical sleeves, gloves, lab coat should be sterile, single use and equipped as recommended by the surgical best practices.

The requested text was added (lines 163-169).

* 2.2: >Isoflurane allows anaesthesia but not analgesia (!), authors should mention the use of proper analgesic prior incision and not only after surgery.< Application of betadine should be the last step prior surgery since it is a much better and more persistent disinfectant than 70% ethanol. If any reason, authors should explain why this ethanol step is added (to avoid betadine to stain the tissue?).

We added text for the administration of an analgesic prior to any incision (170-172). An optional note was added to describe why we wipe with ethanol after betadine solution. We do this step because betadine does tend to stain the tissue, but this step also helps prevent any flakes of skin or debris from entering the wound site. We also explicitly discussed this point with our veterinarian staff and changed the text to recommend multiple scrubs (177-178).

* 2.3: On top of a future video showing this, a schematic draw of the incision localisation would be a plus for the reader. >Such technique (making a hole by sectioning pulled skin) is classic for dissection but not recommended for surgery where straight incision is preferred.<

The reviewer is correct that under most scenarios a straight incision is preferred. However, the mammary imaging window is a rigid device with a diameter of 10 mm. We have found we get much better implantation longevity and results if we remove some of the epithelium. A new figure (Figure 1) has been added to better describe the process.

* 2.6: Authors should mention which antibiotic (molecules, dosage, administration way).

We topically apply the triple antibiotic ointment listed in the materials to the surgery site. We modified the text for clarity (line 198).

-3.6: Respiration frequency follow up is a valuable tip but how authors measure the respiration per minute (rpm)? Authors mention to adjust the isoflurane during the imaging session: authors should add reference values (eg. Isoflurane between 0.5-2%), notably the flow rate should be ranged between 0.5-1L/min contrarily to induction where it can be higher (3.2: 2L/min)

The respirations per min are measured by manually counting breaths over a 30 s time period. Additional text was added to clarify this point (line 230).

- 3.5 Authors must provide blueprints, reference or at least schematics of every "custom" part to allow reader to better understand and/or replicate the protocol. Moreover, authors did not mention the microscope setup (inverted, upright?) nor the objectives (magnification, reference).

We added text to better describe the inverted microscope setup and objectives used in this protocol. It should be noted that this technique can be done on either an upright or inverted system. We have successfully used both but the inverted set up minimizes breathing artifacts (Line 447-449). We have also noted that other objectives can be used so long as they have an extended or long working distance.

-7-9: Authors must share a demo dataset and a demo classifier to allow user to better understand, reproduce and train themselves to reach the expected results. This is very important since authors say “For good results, high quality images with discernible fibres and low noise are required”.

An image and classifier model will be uploaded upon resubmission.

-Authors mention that they develop this label-free pipeline “because it gives the broadest potential compatibility with other mouse models”. Authors must show or reference this compatibility. In other words, is strong CFP/GFP/YFP signal from mouse reporter not altering such analysis by aspecific signal passage through blue filter, since their excitation wavelengths are similar?
This is a CRUCIAL point that could be easily addressed by applying the pipeline on any GFP expressing mouse.

This is an excellent point. To address this, we conducted additional experiments with allografts of GFP-labelled cancer cells. We did not have a GFP-mouse up and running within our colony at the time of submission. Regardless, the GFP did not interfere with the ability of the FLIM images to identify the vasculature. It seemed remarkably robust to interference from GFP fluorescence.

Minor Concerns:
-Title: Intravital imaging of endogenous fluorescence enables investigation into the dynamic reciprocity between tumour cells and the extracellular matrix. The title should be changed to reflect more closely what the protocol does, as opposed to what it could do

The title has been altered to more closely describe what the protocol does.

-Over the use described by authors, such technique may be crucial for any intravital study. It provides multiple localisation cues on a new dimension (FLIM) that is really important for any behaviour study within the stroma or not. The authors should stress the polyvalent use of their technique in intravital microscopy because indeed, dextran block a channel, is transient, invasive and not very convenient (an extra step to an already difficult and low-throughput technique). Moreover, from an ethical point of view, any technique that allows to reduce mouse manipulation (such injection of dextran) is valuable.

This is an excellent point and we devoted extra text in the introduction toward the problems with fluorescent proteins or injectable dextran and the utility of endogenous fluorescence for intravital image analysis (lines 87-104).

-Page 4 (line 89). While tumour cells are typically considered metabolically more active, and therefore there is an expectation that NAD(P)H to fluoresce at a higher intensity, this will likely vary from tumour to tumour (and indeed between different regions within the same tumour). Including an example of the NAD(P)H signal intensity in the normal mammary epithelium would be helpful as a negative control, as well as a discussion (and relevant citation(s) as necessary) to the range that might be expected.
Can this approach be used to identify early, pre-malignant tumour cells/lesions?

Once again, this is an excellent point and indeed the use of NAD(P)H FLIM has been demonstrated to vary within tumors and be useful to distinguish normal vs malignant lesions in prior work published by members of our group (Cell Biochem Biophys. 2009;53(3):145-57. doi: 10.1007/s12013-009-9046-7).

For this manuscript, we want to keep it focused on using autoflourescent sources to compartmentalize intravital images. The purpose here is to simply provide a means to gate or threshold an image to compartmentalize the different microenvironments of the tumor. We have used genetic tumor models and numerous cell lines for xenografts. In all our experience, NADH, while sometimes variable, always provided a means to demarcate the boundaries of the tumor. We, therefore, want to restrict our talking points about that rather than expand upon its utility as a metabolic tool.

-1.3: Ethanol cleaning, especially for only 1 minute, would be better called "quick disinfection" than "sterilization" (autoclaving, dry hoven, ethylene oxide, ...). This should be rephrased. In this purpose, why authors use 100% ethanol instead of 70% ethanol that is known to display higher disinfection property?

We change the text to read that it is a quick disinfection rather than sterilization. We also changed it to read 70% ethanol.

-2.4: Authors should help reader by estimating the incision length to make Ø10mm hole (2r*pi / 2?) The incision length should be 10 mm. We modified the text to clarify that.

-3.1: This tip about thermal expansion is a very valuable advice.

We would like to thank this reviewer for their kind words. This tip is indeed helpful, especially when an immersion media is used. It is less important if you are using an air objective.

-3.2 Add "isoflurane" after 2%. "...with anesthesia machine settings of 2% isoflurane and..."
The text has been modified (line 212).

-3.3 Authors should precise the solution used for MIW cleaning (ethanol? water?)
We use sparkle glass cleaner on a cotton applicator. It only touches the glass and the metal collar protects the surrounding skin. The text has been modified for clarity on this point and it has been added to the table of materials.

-4.3. Representative pictures of the different layers (solitary cells, collagen fibres, poor signal) would be helpful for the reader and during imaging.

We have added a new figure to show how the tumor and collagen change with depth (Figure 1).

-4.4: What is the point to adjust laser intensity/PMT in 4.3 at dwell time of 4µs to readjust it just after with 8µs? In 4.3, could not be better to preview in "gross mode" with low laser and high PMT (very noisy but low exposure) and just spend time to setup high quality imaging in 4.4 with optimal laser intensity/PMT?

We appreciate this comment as it helps with the clarity of our text. In 4.3, the use of low laser intensity and dwell time is to preview the field of view and setup for the high-quality image in 4.4. We added a note to clarify this point. (line 250-251)

-4.5: About the time interval, a mention about the z-step interval and the picture dimensions (pixels x pixels) would also be useful.
Considering microscopy advice, especially for scanning confocal beginners, a short tip-box about how to estimate the smallest time interval per field (z-steps * x_resolution * w_resolution * dwell_time * averaging) would be great. Indeed, for multiple large 3D stacks, 10 minutes can be quickly unreachable (with the authors settings, a 1024*1024*60 3D stack would already take more than 8 minutes to acquire, banning a second position)

The time interval depends entirely on the goals of the experiment. Longer dwell times produce better images, but anything above 8 µs seems to put you at high risk for photo damage. This, of course, is dependent on specific power settings and absorption or scattering of the specific tissue. We view this as a generally safe maximum value. While I agree that the tip box would be useful for beginning users, this technique requires prior microscopy training, and that information will likely not be helpful to most readers. In fact, intravital imaging is a very advanced technique that should not be attempted without some

prior expertise in two-photon or confocal microscopy, which would include expertise in imaging parameter optimization.

-7-9: These parts could only be review upon demo dataset sharing but is theoretically correct.
If authors now how to do it, a ready-to-use ImageJ macro for these processing pipelines would be very useful and easily scalable to single-z, z-stack or max projections.

While having a macro would be useful, we have found macros require extensive optimization and may depend on the user-defined microscopy parameters. Therefore, we currently do not have refined macros that are suitable for broad dissemination. Rather, we have a streamlined workflow which we presented. As this technique is used more in the lab, a script will be written and we will share via the lab website.

- Figures could be better represented and annotated.
* Figure legends refer to arrows, gold stars, red triangles which are not represented on the PDF.

The figures have been revised to improve representation of the protocol. The gold stars and red triangles were missing; An older version of the figure was uploaded accidently, which has now been corrected.

* Authors should add on Figure 1 the signal origin to stress that is is label-free imaging (eg. Collagen (SHG)).

Figures 1 and 2 have been revised and labeled to stress the signal origin. We have also stressed this point in the figure legends and text.

* Authors should add merged image of E and F to better see (miss)matches of label-free FLIM imaging and classical dextran imaging.

An additional panel with a merged image was added to the figure.

* Authors should reconsider the Table 1 representation to a classic histogram plot showing FOV as individual dot (Y: Area ratio, X: mice).

The data shown in the table has now been formatted into a dot plot and included into the updated Figure 2.

-Authors must add short result-dedicated methods embedded in the text to explain at least, when the dextran was injected (hopefully, after label-free images acquisition to exclude cross-signals), its molecular weight and its fluorophore as like the microscope setup.

Additional text was added to the manuscript to better describe the approach for our comparison. The fluorescent dextran was also added to the material sheet.

-Image restoration through machine-learning is a trendy topic, being progressively implemented within microscope softwares.
* Considering 1E and 1F, it is fairly imaginable to retrieve dextran imaging quality through FLIM layer (see CSBDeep) - training pairs FLIM/Scanning
* This can also drastically reduce FLIM acquisition time - training pairs shortFLIM/longFLIM
* And maybe both - training pairs shortFLIM/Scanning
Since these aspects are currently presented as limiting points of authors technique, it is also important to mention and discuss that these may be easily overcome through fast post-processing.

We strongly agree with the reviewer on this point and have given it extensive thought. A few lines of additional text have been added to the discussion to address this point (lines 671-679).

training dataset

Click here to access/download;Supplemental File (Figures, Permissions, etc.);MAX_NADHlifetime_750nm_ms311_FOV1.tif

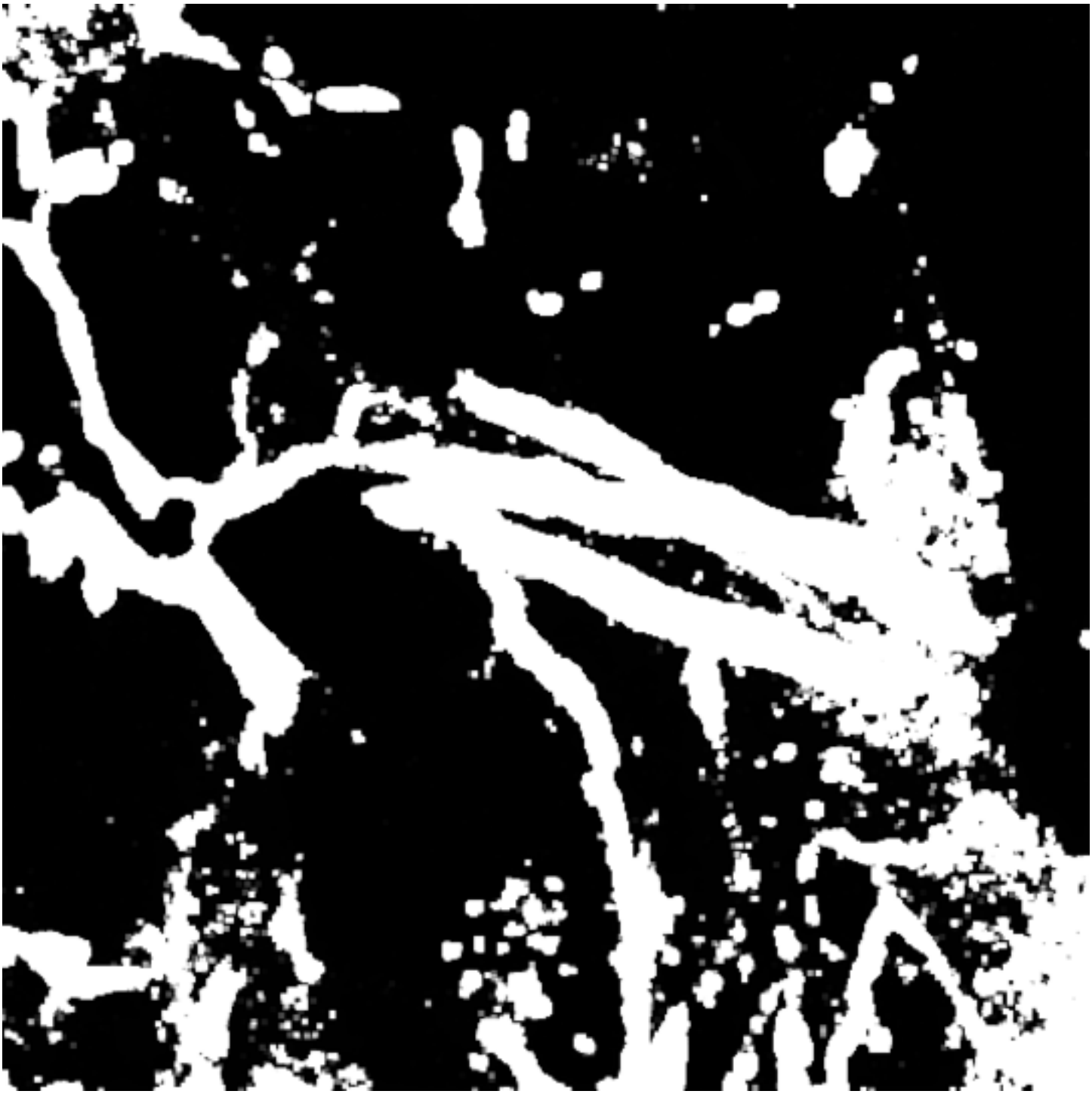

classifier model